ISSN 1063-7710, Acoustical Physics, 2019, Vol. 65, No. 1, pp. 123–131. © Pleiades Publishing, Ltd., 2019.

ACOUSTICS OF LIVING SYSTEMS. BIOMEDICAL ACOUSTICS

Generalized Sidelobe Canceller for Ultrasound Imaging based on Eigenvalue Decomposition[1]

Ping Wang[a], *, Yizhe Shi[a], Jinyang Jiang[a], Lu Kong[a], and Zhihui Gong[a]

[a]*State Key Lab. of Power Transmission Equip. and System Security and New Tech., Chongqing University, Chongqing, 400044 China*

**e-mail: cqu_dqwp@163.com*

Received November 30, 2017; Revised May 21, 2018; Accepted August 28, 2018

Abstract—The improved generalized sidelobe canceller (GSC) based on eigenvalue decomposition beamforming technique for ultrasound imaging is proposed. Firstly, the signal subspace is obtained by performing eigenvalue decomposition on the covariance matrix of received data. Secondly, the weighting vector of GSC is divided into adaptive and non-adaptive two parts. Then the non-adaptive part is projected into the signal subspace to obtain a new steer vector. Subsequently, based on the orthogonal complementary space of the new steer vector, the blocking matrix is constructed. Finally, the weighting vector is updated by projecting the final weighting vector into the signal subspace. In order to verify the proposed algorithm, the simulations of the point targets and the cyst phantom were conducted in Field II. The experimental results indicate that the proposed method has better resolution and contrast ratio than the conventional algorithms. In addition, the algorithm is robust to noises. Furthermore, combining with coherence factor, the contrast ratio of the proposed algorithm can be further improved in comparison with a conventional GSC with coherence factor.

Keywords: generalized sidelobe canceller, eigenvalue decomposition, resolution, contrast ratio, robustness

DOI: 10.1134/S1063771019010159

1. INTRODUCTION

Ultrasound is widely used in medical and industrial inspection field due to its safety and low cost. The transducer array transmits a focused beam to the target and receives the pulse-echo dynamically to form a B-mode image. The conventional delay-and-sum (DAS) beamforming is the most widely used and the simplest method in ultrasound imaging, but it has many drawbacks, such as low resolution, serious artifacts and grating sidelobes. The adaptive beamforming techniques can overcome some of these defects. J.F. Synnevag [1] adopted the minimum variance (MV) adaptive beamforming method, which was first proposed by Capon in 1969, in medical ultrasound imaging field and achieved a better image quality than DAS. Although the MV method can achieve a better resolution, its robustness is not better than the conventional DAS [2]. J. Li [3] used the diagonal loading method to improve the beamformer's robustness and provided a guidance to define the amount of diagonal loading. K.W. Hollman first put forward the conception of coherence factor (CF) which can effectively compress the sidelobes to improve the contrast ratio of imaging [4], and this method is adopted in many adaptive algorithms to correct the phase distortion resulted from the focusing error [5–7]. Besides, Li et al. proposed a generalized coherence factor (GCF) as an adaptive weighting coefficient for imaging algorithms, which is widely used in practice [8, 9]. Many scholars seek other ways to improve the lateral resolution and SNR except the MV-based methods. In [10], the author improved the image quality via using the phase information, phase coherence factor (PCF) and sign coherence factor (SCF). Apart from the conventional DAS imaging algorithm, almost all of improved methods will increase the computational complexity. Asl and Mahloojifar suggested that the computational complexity of matrix inversion can be reduced by constructing the covariance matrix into a Toeplitz matrix [11]. Some scholars also proposed the QR decomposition method to realize the fast inversion calculation of the covariance matrix [12]. Other MV-based computation reduction methods can be found in [13, 14]. The generalized sidelobe canceller (GSC) algorithm, as the equivalent structure of MV, is divided into the upper and lower channels. The upper channel is a non-adaptive channel and the lower channel is the adaptive part; the desired signal can be blocked by the blocking matrix [15–17]. At last, the undesired signal is eliminated and the quality of ultrasound imaging is improved through overlaying.

This paper proposes an improved generalized sidelobe canceller beamforming (IGSC) differing from [18]. The proposed method concerns more about the improvement of resolution and contrast ratio (CR). Based on IGSC, the IGSC-CF algorithm is also pro-

[1] The article is published in the original.

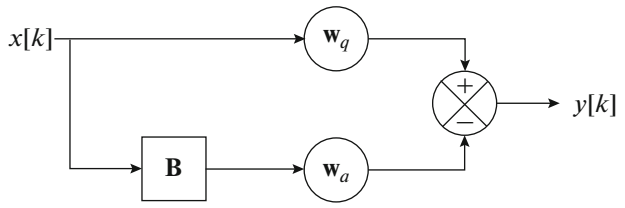

Fig. 1. Generalized sidelobe canceller.

posed in order to further compress sidelobes and improve the contrast ratio of imaging. The main feature of the proposed method is to modify the blocking matrix, instead of defining it fixed beforehand. Then the non-adaptive weighting vector is projected into the signal space to acquire a new steer vector, and the improved blocking matrix is constructed based on its orthogonal complementary space adaptively. At last, the final weighting vector is projected into the signal space to get a new vector to further improve the performance of the algorithm. The proposed algorithm in this paper can be applied to synthetic, plane wave and other acquisition sequences.

This paper is organized as follows: the IGSC method is presented in section 2 in detail. The procedures of acquiring the covariance matrix are described in section 3. Experimental results and the discussion of the resolution, CR and robustness are presented in section 4, which includes the comparison between the proposed IGSC, IGSC-CF, and DAS, MV, GSC, GSC-CF as well. All experiments use the linear array for the transmission and reception of ultrasound signals. Conclusion is drawn in section 5.

2. METHOD

2.1. Generalized Sidelobe Canceller

The MV is the most commonly-adopted adaptive beamforming technique. Supposing a linear array which consists of N equal space elements, its beamforming output can be written as

$$y[k] = \frac{1}{N}\sum_{i=1}^{N} w_i x_i(k) = \frac{1}{N}\mathbf{w}^H[k]\mathbf{x}[k], \tag{1}$$

where $x_i[k]$ is the k-th signal sample received by i-th element after a certain time delay, $\mathbf{w}$ is the weighting vector for each element and $\mathbf{w}^H[k] = (w_1[k], w_2[k].....w_N[k])^H$.

The main task is to obtain the $\mathbf{w}$. A criterion is provided in MV, which the weights are acquired by minimizing the output power of the beamformer subjecting to a constraint condition, it can be expressed as follows:

$$\begin{cases} p[k] = E\left\{|y[k]|^2\right\} = \mathbf{w}^H E\left\{\mathbf{x}[k]\mathbf{x}^H[k]\right\}\mathbf{w} \\ \mathbf{w} = \arg\min \mathbf{w}^H\mathbf{R}\mathbf{w} \quad s.t \quad \mathbf{w}^H\mathbf{a} = 1, \end{cases} \tag{2}$$

where *s.t* is the abbreviation of "subject to", meaning constrained, $p[k]$ is the output power, $\mathbf{R} = E\left\{\mathbf{x}[k]\mathbf{x}^H[k]\right\}$ is the covariance matrix of the received data, $\mathbf{a}$ is the steering vector of the desired signal. The solution to the optimization problem (2) can be obtained by using Lagrangian method, and the solution is:

$$\mathbf{w}[n] = \frac{\mathbf{R}^{-1}[n]\mathbf{a}}{\mathbf{a}^H\mathbf{R}^{-1}[n]\mathbf{a}}. \tag{3}$$

The GSC is the equivalent structure of the MV algorithm. Unlike MV, the GSC algorithm transforms its constraint optimization problem into unconstrained optimization problem through the upper and lower branches, and its structure is illustrated in Fig. 1.

In GSC, the weighting vector is divided into non-adaptive and adaptive parts, the first one lies in the constraint subspace and the latter belongs to the subspace, which is orthogonal to the former. The weighting vector can be expressed as

$$\mathbf{w} = \mathbf{w}_q - \mathbf{B}\mathbf{w}_a \quad s.t \quad \mathbf{B}^H\mathbf{w}_q = 0, \tag{4}$$

where $\mathbf{w}_q$ is a $N \times 1$ fixed vector and $\mathbf{B}$ is a $N \times (N-1)$ blocking matrix, which blocks the desired signal into the lower path. Since the $\mathbf{w}_q$ is fixed, the previous constraint problem (2) turns into an unconstrained optimization problem to solve the adaptive vector $\mathbf{w}_a$. The optimal solution is [19]:

$$\mathbf{w}_a = \left(\mathbf{B}^H\mathbf{R}\mathbf{B}\right)^{-1}\mathbf{B}^H\mathbf{R}\mathbf{w}_q. \tag{5}$$

Here denoting $y_c = \mathbf{w}_q^H\mathbf{x}[k]$, $z = \mathbf{B}^H\mathbf{x}[k]$ is the output after the received data $x_i[k]$ passes through the upper branch and the blocking matrix $\mathbf{B}$ respectively. The adaptive weighting vector can be expressed as:

$$\mathbf{w}_a = \mathbf{R}_z^{-1}\mathbf{p}_z, \tag{6}$$

where $\mathbf{R}_z = \mathbf{B}^H\mathbf{R}\mathbf{B}$, $\mathbf{p}_z = \mathbf{B}^H\mathbf{R}\mathbf{w}_q$, $\mathbf{R}_z$ is the covariance matrix of z and $\mathbf{p}_z$ is the correlation vector of y_c and z. In fact, the optimal solution (5) is the Wiener solution that minimizes the mean square error between the upper and lower paths.

2.2 Eigenvalue Decomposition

According to the echo signals, the covariance matrix can be obtained:

$$\mathbf{R}(k) = \varepsilon\{\mathbf{x}(k)\mathbf{x}(k)^H\}, \tag{7}$$

where $\varepsilon\{\cdot\}$ represents the expected value, $\mathbf{x}(k) = [x_0(k), x_1(k), \ldots, x_{N-1}(k)]^H$, N is the number of array elements, k represents the k-th sampling point and $\mathbf{x}(k)$ is the echo data of the k-th sampling point received by all array elements.

In practical applications, the covariance matrix is usually unknown. Therefore, spatial smoothing is generally used to estimate the covariance matrix with autocorrelation sampling matrix, to effectively reduce the matrix dimension and eliminate the correlation between echo signals:

$$\hat{\mathbf{R}}(k) = \frac{1}{N-L+1}\sum_{l=1}^{N-L+1} x_n^l(k)x_n^l(k)^H. \quad (8)$$

In equation (8), N is the number of array elements, L is the number of array elements in the sub-array, all array elements can be divided into $(N-L+1)$ sub-arrays altogether. The average of the echo data of each sub-array can be used to estimate the covariance matrix.

After obtaining the signal covariance matrix $\mathbf{R}$, the space $\mathbf{U}$ is obtained by using eigenvalue decomposition, which includes both the desired signal and the noise signal space. Then, rearranging its eigenvalues λ_i in descending order, if the ratio of adjacent eigenvalue $\lambda_i / \lambda_{i+1}$ exceeds a preset threshold value, a new space is constituted:

$$\mathbf{U}_s = [\mathbf{u}_1, \mathbf{u}_2 \ldots\ldots \mathbf{u}_i], \quad (9)$$

where $\mathbf{u}_i$ is the corresponding eigenvector and $\mathbf{U}_s$ is the signal space.

In order to increase the robustness of the algorithm, the diagonal loading technique is used to process the matrix, $\hat{\mathbf{R}}(k) + \varepsilon\mathbf{I}$ is used instead of the original autocorrelation matrix $\hat{\mathbf{R}}(k)$, where $\mathbf{I}$ is the unit matrix and the diagonal loading coefficient is $\varepsilon = \text{trace}(\hat{\mathbf{R}}(k))\delta$, δ is a constant satisfying $\delta \le \frac{1}{L}$. In this paper $\delta = \frac{1}{100L}$.

2.3. Improved Generalized Sidelobe Canceller

The GSC can work properly whether z contains a little desired signal or not. Once the desired signal exceeds its limitation, which means the desired signals leak much to the lower path, thus the imaging quality will degrade a lot. Here the IGSC is introduced by modifying the blocking matrix $\mathbf{B}$ and the final weighting vector is projected into the signal space to improve the GSC ability to block the undesired signal. As described in (4), the blocking matrix $\mathbf{B}$ is orthogonal to the non-adaptive weighting vector $\mathbf{w}_q$. In the proposed IGSC, the new adaptive vector $\mathbf{w}_p$ is obtained by projecting the non-adaptive vector $\mathbf{w}_q$ into the signal space $\mathbf{U}_s$, and the improved blocking matrix $\mathbf{B}_p$ is orthogonal to the adaptive vector $\mathbf{w}_p$. The specific description is shown in (10), through these operations, the blocking matrix changes from a non-adaptive matrix into an adaptive matrix, which improves the ability to block the desired signal.

The new steer vector is acquired by projecting the non-adaptive weighting vector into the signal space:

$$\boldsymbol{w}_p = \mathbf{U}_s\mathbf{U}_s^H\mathbf{w}_q \quad s.t \ \mathbf{B}_p^H\mathbf{w}_p = 0. \quad (10)$$

The renewed blocking matrix $\mathbf{B}_p$ is then established on the basis of the orthogonal complementary space of $\mathbf{w}_p$. Thus the weighting vector can be expressed as

$$\mathbf{w} = \mathbf{w}_q - \mathbf{B}_p\mathbf{w}_a^p, \quad (11)$$

where $\mathbf{w}_a^p = \left(\mathbf{B}_p^H\mathbf{R}\mathbf{B}_p\right)^{-1}\mathbf{B}_p\mathbf{R}\mathbf{w}_q$.

In general, $\mathbf{w}_q$ is a $N \times 1$ fixed vector and the blocking matrix $\mathbf{B}$ is orthogonal to vector $\mathbf{w}_q$, so $\mathbf{B}$ is usually a fixed matrix. In this paper, we project $\mathbf{w}_q$ into the signal space and then construct the blocking matrix $\mathbf{B}$ adaptively.

Here the blocking matrix is established in a novel way, and then the final weighting vector is obtained that can be projected into the signal space to further improve the resolution and contrast ratio. So, the final weighting vector can be expressed as:

$$\mathbf{w}_{\text{opt}} = \mathbf{E}_s\mathbf{E}_s^H\mathbf{w}. \quad (12)$$

After obtaining the covariance matrix and the result from (12), the IGSC beamforming output can be determined as:

$$y[k] = \frac{1}{N-L+1}\sum_{i=1}^{N-L+1} w_{\text{opt},i}^H[k]\,x_i[k]. \quad (13)$$

By emphasizing the in-phase signals and reducing the out-of-phase ones, CF can be weighted to improve the contrast ratio, enhance the ability of sidelobe suppression. The definition of CF is the ratio of coherent energy to total energy, the expression is as follows:

$$CF[k] = \frac{\left|\sum_{i=1}^{N-L+1} x_i(k)\right|^2}{(N-L+1)\sum_{i=1}^{N-L+1}\left|x_i(k)\right|^2}. \quad (14)$$

In order to make an overall comparison with [18], the proposed method integrates with CF too, the output of combining IGSC with CF is

$$y[k] = \frac{CF[k]}{N-L+1}\sum_{i=1}^{N-L+1} w_{\text{opt},i}^H[k]\,x_i[k]. \quad (15)$$

Table 1. Initial values for the experiment

Parameter		Value
Central frequency	f_0	3.5 MHz
Sampling frequency	f_s	50 MHz
Array type		Linearly
Transducer number	N	64
Subarray length	L	32
Bandwidth	B	0.6 mm
Element width		0.2 mm
Element height		5 mm
Element spacing		0.48 mm
Focal depth (points)		60 mm
Focal depth (cyst)		25 mm

4. EXPERIMENTAL RESULTS

This section tested the performance of DAS and other adaptive algorithms, as well as the proposed methods IGSC and IGSC-CF based on Field II [20, 21]. We conducted the experiment with two kinds of detection objects, the first one consists of 18 point targets uniformly distributed between 30 to 70 mm in two columns, and the second is a circular cyst in a speckle medium. The basic parameters setting for these experiments are displayed in Table 1. It should be noted that all the methods have used the spatial smoothing and diagonal loading technique. Besides, a Gaussian white noise with a certain signal-to-noise ratio has been added to each simulation experiment [22]. The simulation of this paper adopts the linear array transducer to transmit ultrasound signals and the dynamic range of all images is 80 dB.

4.1. Point Targets Experiment

The point targets are distanced 4 mm in the lateral and 5 mm in the axial directions, images through different methods are displayed in Fig. 2. It can be seen that the IGSC-CF has the best performance and all adaptive methods have better performance than DAS. GSC performs nearly the same as MV. After combining with CF, some artifacts in images are removed. The proposed IGSC achieves similar results in the further scanning depth, while it performs slightly worse than the GSC-CF within the 45 mm, but better than the GSC. This is because CF weighting can improve the contrast ratio and resolution by emphasizing the in-phase signals and reducing the out-of-phase ones.

After combining the IGSC with CF, both the near area and the farther depth can acquire better resolution than other methods. This improvement can be further verified by Figs. 3a and 3b depicting the lateral variation at depth of 40 and 60 mm respectively.

It can be seen from Fig. 3a that DAS image has the greatest sidelobe level, GSC and MV improve slightly, however the imaging effect has a significant improve-

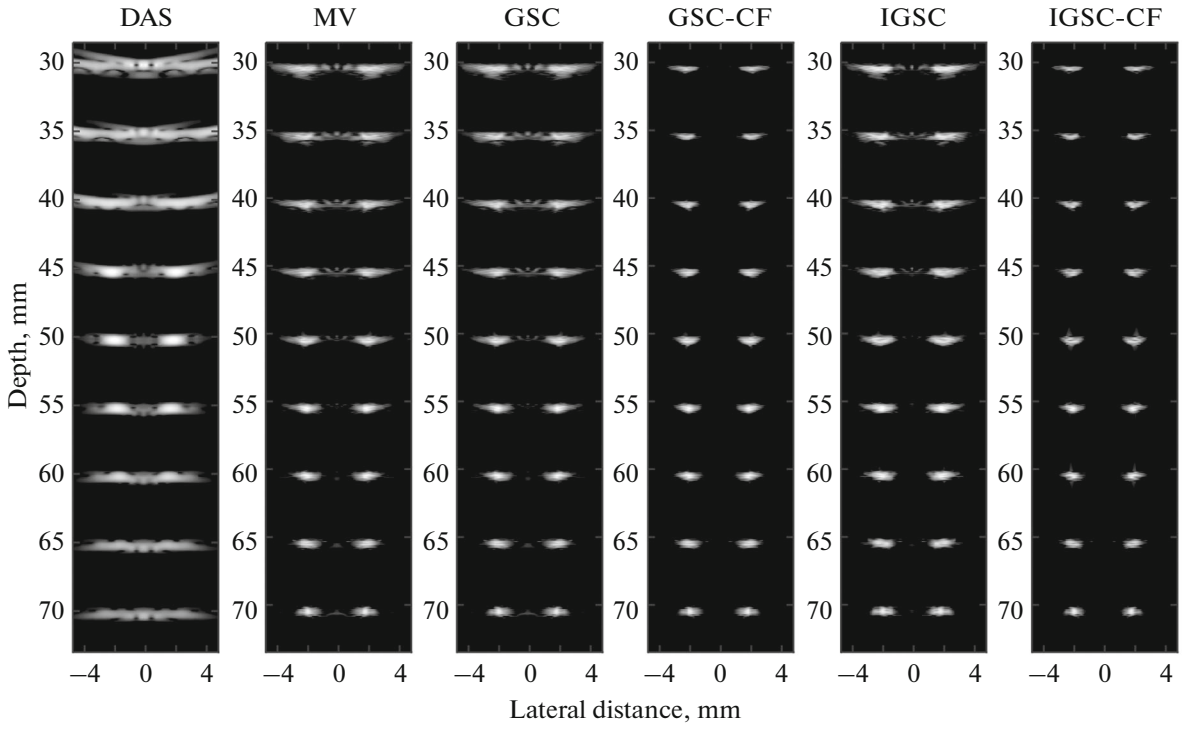

Fig. 2. 18-point targets images obtained using different methods.

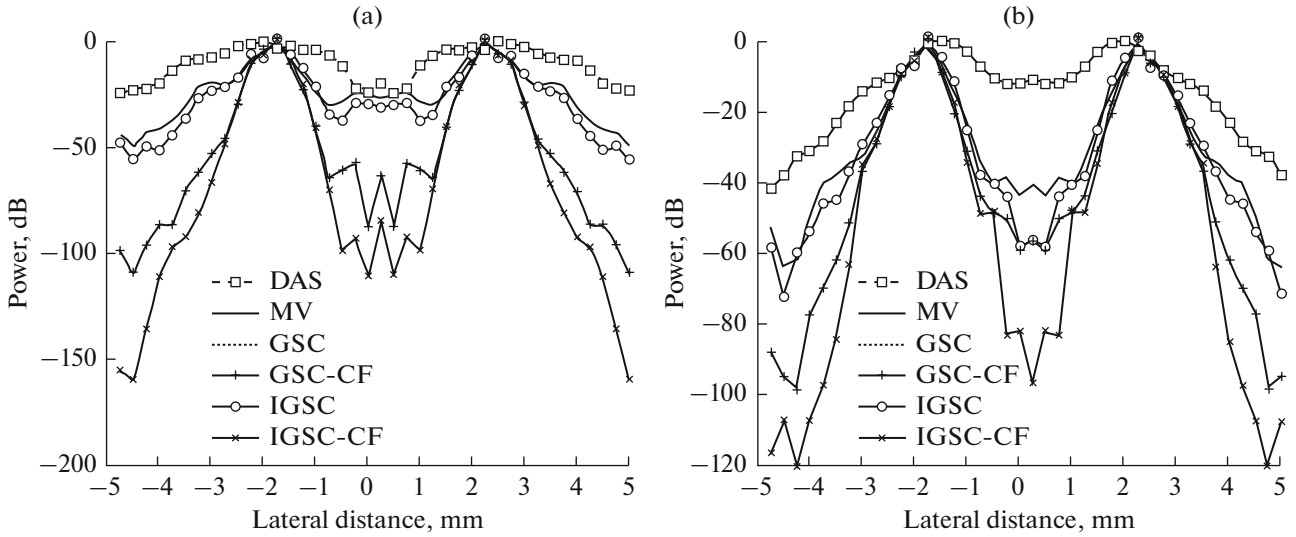

Fig. 3. (a) Lateral variation at depth of 40 mm, (b) lateral variation at depth of 60 mm.

ment with the help of CF, IGSC has a little improvement on the basis of GSC and has significant improvement after combining with CF. Besides, IGSC-CF performs better than GSC-CF. Here we use −6 and −20 dB mainlobe width as indications of resolution and use the first sidelobe peak to represent the contrast ratio. As it can be seen from Table 2, the IGSC performs slightly better than GSC at −20 dB mainlobe width, while it behaves 0.37 mm over GSC. IGSC-CF has similar results at −6 and −20 dB mainlobe width comparing with GSC-CF, but it is more advantageous at lower dB values than GSC-CF. The last column shows the contrast ratio of the different methods, and lower quantities represent better image quality. The proposed IGSC performs better than MV and GSC, but worse than GSC-CF, the reason is that CF has great ability in suppressing the sidelobes. So, the image quality of IGSC-CF is far superior to other methods.

Similar patterns are shown in the case of the farther scanning depth (Fig. 3b), while the advantages of the proposed methods appear. Similarly, the DAS performs the worst and the IGSC has similar mainlobe width with MV and GSC, but when these methods are combined with CF, the first sidelobe peak can be greatly reduced. On the other hand, the first sidelobe peak of IGSC is around 20 dB better than that of GSC and MV, which indicates that the proposed method has better ability to compress sidelobes. When combined with CF, the contrast ratio has significant improvement on the basis of IGSC; moreover, the clutter signals have larger distance to the mainlobe in GSC-CF and IGSC-CF. More experimental results are shown in Table 3.

In order to test the robustness against noises of the proposed methods, a 10 dB white Gaussian noise is added to the received data. Figure 4 displays the images obtained by the abovementioned methods, and Fig. 5 shows the corresponding resolution at depth of 40 and 60 mm respectively. After adding the noises, the background white spots are obviously enhanced. It can be seen that GSC-CF degrades its robustness against noises than DAS, MV and GSC. IGSC has better robustness than other adaptive methods, since

Table 2. Numerical results of mainlobe width for different methods in 40 mm

Method	Mainlobe width		First sidelobe peak, dB
	−6 dB	−20 dB	
DAS	2.18	3.85	−3.02
MV	0.56	2.06	−18.54
GSC	0.56	2.06	−18.54
GSC-CF	0.50	1.09	−57.18
IGSC	0.61	1.69	−28.60
IGSC-CF	0.52	1.14	−84.07

Table 3. Numerical results of mainlobe width for different methods in 60 mm

Method	Mainlobe width		First sidelobe peak, dB
	−6 dB	−20 dB	
DAS	1.28	7.18	−10.75
MV	0.58	1.49	−38.40
GSC	0.58	1.49	−38.40
GSC-CF	0.52	1.28	−55.90
IGSC	0.53	1.55	−55.91
IGSC-CF	0.51	1.31	−81.67

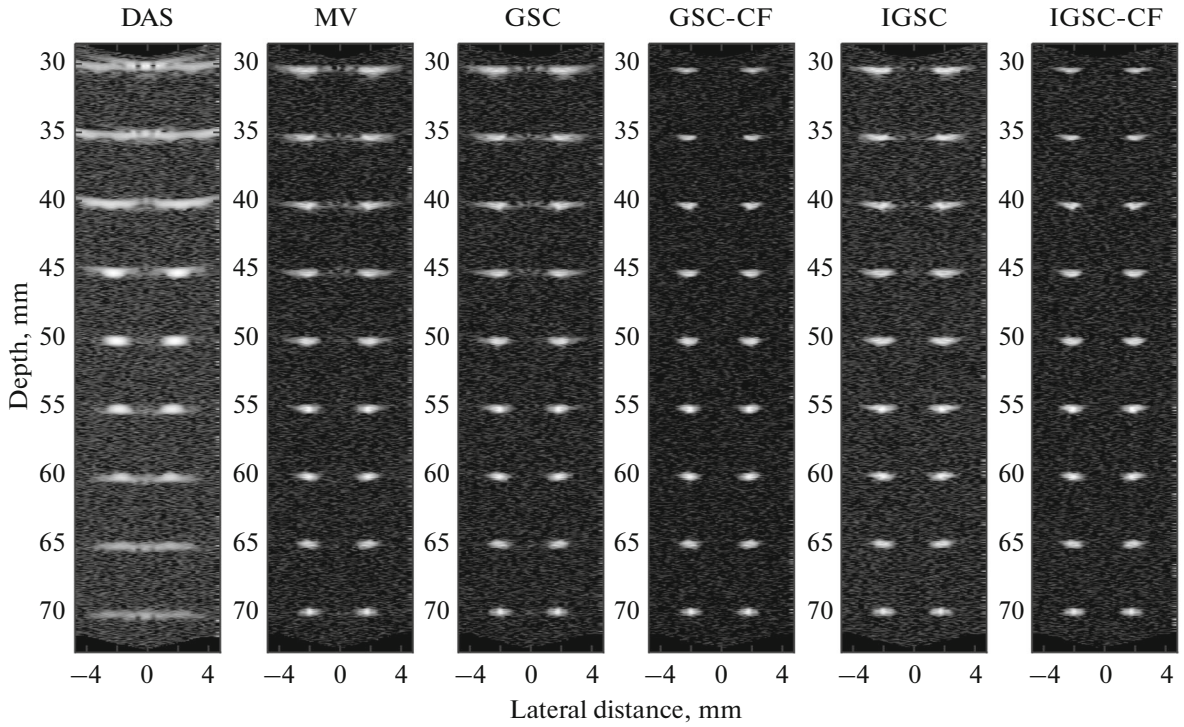

Fig. 4. 18-point targets noise images obtained using different methods.

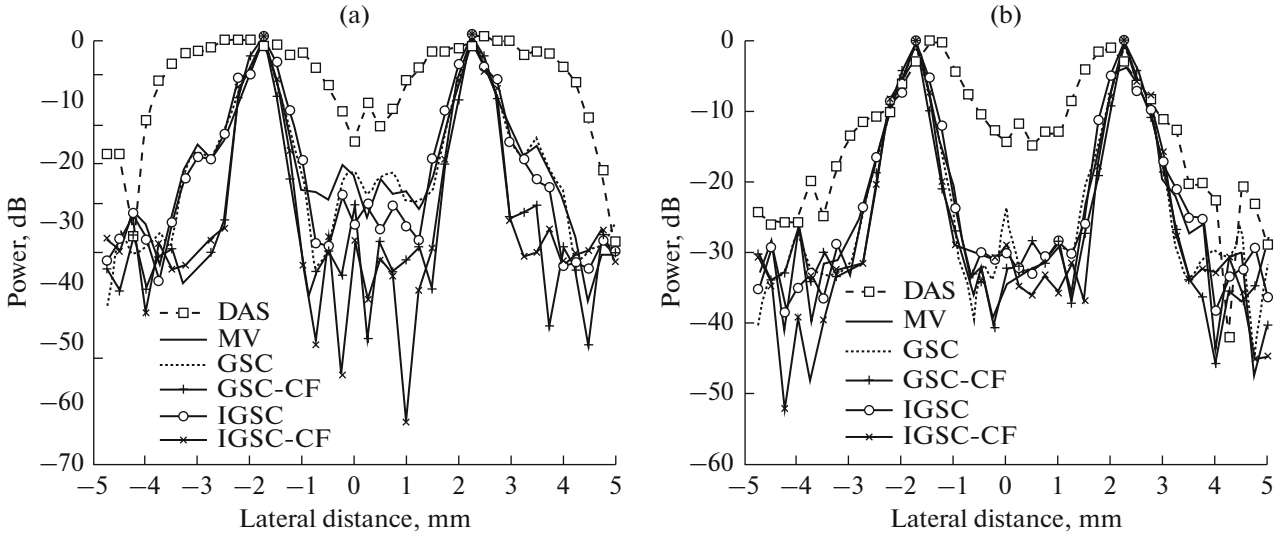

Fig. 5. (a) Lateral variation at depth of 40 mm with noise, (b) lateral variation at depth of 60 mm with noise.

we add relatively strong noises to the echo signals, all methods' performance are degenerated to some degree.

Figure 5a,b display the corresponding resolution at depth of 40 and 60 mm respectively. Both for the 40 and 60 mm, IGSC achieves better first sidelobe peak value than DAS, MV and GSC which shows inferiority to GSC-CF and IGSC-CF in the 40 mm. However, it shows a little dominance over GSC-CF and IGSC-CF in the 60 mm, which illustrates that the IGSC has better robustness than other adaptive algorithms. IGSC has some improvement in mainlobe width after integrating with CF in both 40 and 60 mm. Besides, IGSC displays nearly the same −6 dB mainlobe width and the lower first sidelobe peak value than GSC-CF and IGSC-CF in the farther scanning depth situation. Meanwhile, the IGSC has a lower first sidelobe peak value than DAS, MV and GSC both in the near area and the farther scanning depth, which shows

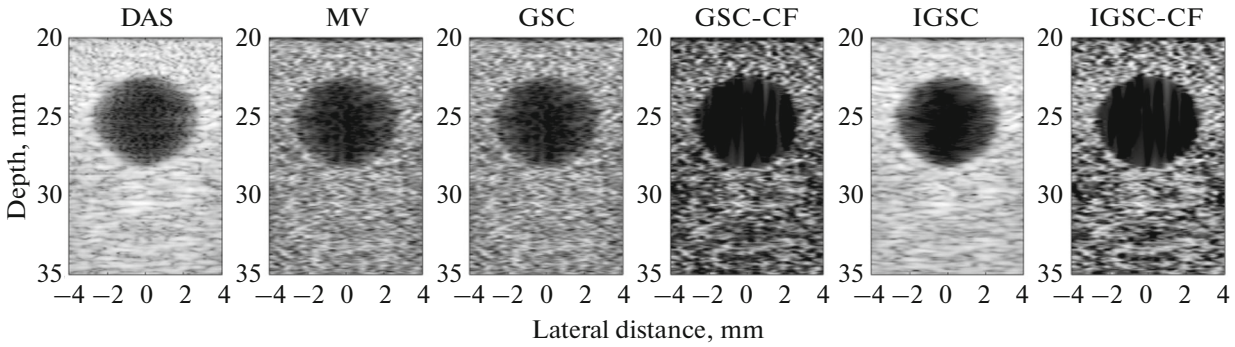

Fig. 6. Cyst phantom images obtained using different methods.

its robustness against noises. The detailed numerical results are listed in Tables 4 and 5.

4.2. Cyst Phantom Experiment

The cyst phantom is set 5 mm radius located at the depth of 25 mm in a speckle medium. The scatter amplitudes are Gaussian distributed. The spatial smoothing and the diagonal loading technique are adopted as well. The specific experiment parameters are listed in Table 1. Images after processing by different methods are shown in Fig. 6. In the same way, a 10 dB noise is added to the received echo signals, and the image results are shown in Fig. 7.

For the purpose of stating the superiority of the proposed methods, we calculated the contrast ratio and contrast-to-noise ratio (CNR). CR is the difference between the value in background and value in circle cyst region, CNR is calculated by CR divided by the standard deviation of image intensity in background region. The standard deviation is the index of robustness of the algorithm [23, 24]. Table 6 illustrates the CR and CNR without noises, and Table 7 describes the indexes under noise occasions.

As can be seen from Table 6, the MV and GSC perform almost the same without noise, and the proposed IGSC performs better than MV, GSC and GSC-CF. With the help of CF, both GSC and IGSC have significant improvement in CR. From the view of robustness, the DAS performs the best and the proposed IGSC-CF sacrifices the robustness to some extent. For CR, IGSC-CF do the best, which means the proposed IGSC-CF performs better than GSC-CF overall, and the IGSC also performs better than GSC and MV overall. From Table 7 we can see that the CR and CNR of all algorithms have reduced significantly under the circumstance of relatively strong noises, which shows that noise has a greater impact on the imaging results of adaptive algorithms. Besides, both the mean value in cyst region and the mean value in background region have a certain degree of increasing due to noises. The proposed IGSC has higher CR than other methods except DAS, which means that it has a stronger ability to suppress noises than the other methods and has the best robustness compared with other adaptive algorithms. GSC-CF shows the lowest CR, this is because CF raises the standard deviation of the background region and the robustness of the algorithm is reduced. At last, the DAS behaves the best in CR, which shows that it has the best robustness mainly due to the simplest operation of this method. In contrast, the adaptive algorithms are more susceptible to noises due to the more complex matrix operations than the DAS, so the robustness of the algorithm is also reduced. For standard deviation, the proposed IGSC is more robust than other adaptive algorithms

Table 4. Numerical results of mainlobe width for different methods in 40 mm with noise

Method	Mainlobe width		First sidelobe peak, dB
	−6 dB	−20 dB	
DAS	2.36	8.76	−2.19
MV	0.56	1.60	−17.52
GSC	0.54	1.67	−16.54
GSC-CF	0.51	1.06	−27.74
IGSC	0.59	1.73	−25.98
IGSC-CF	0.53	1.09	−28.40

Table 5. Numerical results of mainlobe width for different methods in 60 mm with noise

Method	Mainlobe width		First sidelobe peak, dB
	−6 dB	−20 dB	
DAS	1.19	6.83	−11.46
MV	0.57	1.58	−25.77
GSC	0.56	1.49	−23.10
GSC-CF	0.49	1.25	−26.04
IGSC	0.50	1.52	−28.30
IGSC-CF	0.48	1.26	−26.04

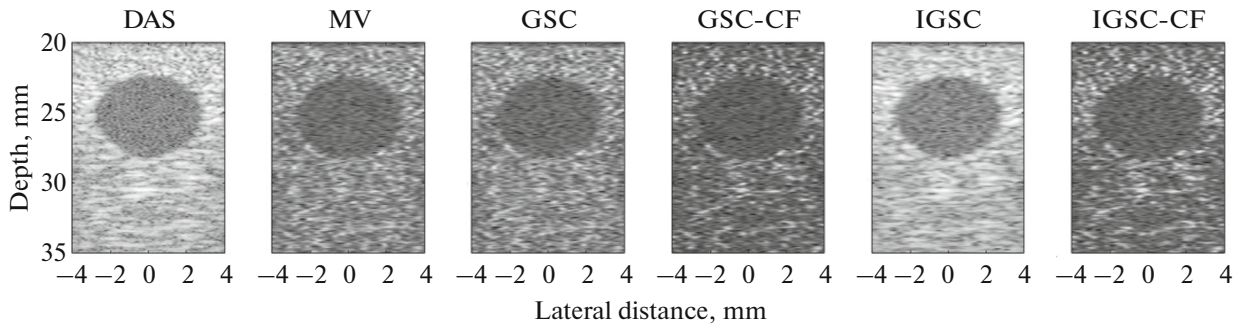

Fig. 7. Cyst phantom noise images obtained using different methods.

Table 6. CR and CNR of the cyst phantom through different methods

Method	Mean value in cyst region, dB	Mean value in background region, dB	Standard deviation	CR	CNR
DAS	−37.16	−17.68	6.81	19.48	2.86
MV	−47.21	−26.79	12.84	20.42	1.59
GSC	−47.21	−26.79	12.84	20.42	1.59
GSC-CF	−57.24	−35.35	16.42	21.89	1.33
IGSC	−46.21	−16.90	13.24	29.31	2.21
IGSC-CF	−55.89	−25.94	17.16	29.95	1.75

Table 7. CR and CNR of the cyst phantom through different methods with noise

Method	Mean value in cyst region, dB	Mean value in background region, dB	Standard deviation	CR	CNR
DAS	−24.35	−14.09	6.39	10.26	1.61
MV	−32.58	−24.46	8.05	8.12	1.01
GSC	−32.35	−24.28	8.06	8.07	1.00
GSC-CF	−36.49	−30.31	8.68	6.18	0.71
IGSC	−25.41	−15.29	6.84	10.12	1.48
IGSC-CF	−29.74	−21.82	8.49	7.92	0.93

and the proposed IGSC-CF is more stable than the GSC-CF.

5. CONCLUSIONS

This paper proposes an improved generalized sidelobe canceller (IGSC) in ultrasound imaging system, which constructs the blocking matrix in a novel way and projects the final weighting vector into signal space. This method gets an adaptive blocking matrix that increases the ability of the adaptive part to block the desired signal. The experimental results of the point targets image and the cyst phantom image show that the main feature of the proposed method can enhance the mainlobe width, first sidelobe peak and CR compared with DAS, MV and GSC. Seeing from standard deviation of cyst phantom experiment, the IGSC has stronger robustness compared with other adaptive algorithms. When IGSC is integrated with CF, not only the resolution, but also the CR are improved as well. On the other hand, when exposed in noises occasions, the proposed IGSC has better robustness than MV, GSC, GSC-CF and IGSC-CF, and DAS has the best robustness compared to adaptive algorithms because of its minimal complexity. Although the robustness of IGSC is degenerated to some degree after combining with CF, it still performs better than GSC-CF, which further validates the effectiveness and practicability of the proposed method.

ACKNOWLEDGMENTS

This study was supported by NSFC Grant no. 51677010.

REFERENCES

1. J. F. Synnevag, A. Austeng, and S. Holm, IEEE Trans. Ultrason., Ferroelectr. Freq. Control **54** (8), 1606 (2007).
2. A. G. Sazontov and A. I. Malekhanov, Acoust. Phys. **61** (2), 213 (2015).
3. J. Li, P. Stoica, and Z. Wang, IEEE Trans. Signal Process. **51** (7), 1702 (2003).
4. Tingting Liu, Hao Zhou, Yinfei Zheng, J. Acoust. **40** (6), 855 (2015).
5. P. C. Li and M. L. Li, IEEE Trans. Ultrason., Ferroelectr. Freq. Control **50** (2), 128 (2003).
6. M. L. Li, W. J. Guan, and P. C. Li, IEEE Trans. Ultrason., Ferroelectr. Freq. Control **51** (1), 63 (2004).
7. A. A. Tsukanov and A. V. Gorbatikov, Acoust. Phys. **64** (1), 70 (2018).
8. S. Park, A. B. Karpiouk, and S. R. Aglyamov, in *Proc. IEEE Int. Ultrasonics Symposium (IUS)* (Beijing, 2008), p. 1088.
9. B. M. Asl and A. Mahloojifar, IEEE Trans. Ultrason., Ferroelectr. Freq. Control **56** (9), 1923 (2009).
10. J. Camacho, M. Parrilla, and C. Fritsch, IEEE Trans. Ultrason., Ferroelectr. Freq. Control **56** (5), 958 (2009).
11. B. M. Asl and A. Mahloojifar, IEEE Trans. Ultrason., Ferroelectr. Freq. Control **59** (4), 660 (2012).
12. J. Park, S. M. Wi, and J. S. Lee, IEEE Trans. Ultrason., Ferroelectr. Freq. Control **63** (2), 256 (2016)
13. X. Zeng, Y. Wang, J. Yu, and G. Yi, IEEE Trans. Ultrason., Ferroelectr. Freq. Control **60** (12), 2670 (2013).
14. B. M. Asl and A. Mahloojifar, IEEE Trans. Ultrason., Ferroelectr. Freq. Control **59** (4), 660 (2012).
15. C. C. Nilsen and I. Hafizovic, IEEE Trans. Ultrason., Ferroelectr. Freq. Control **56** (10), 2187 (2009).
16. J. F. Synnevag, A. Austeng, and S. Holm, IEEE Trans. Ultrason., Ferroelectr. Freq. Control **54** (8) 1606 (2007).
17. Jiake Li, Xiaodong Chen, Yi Wang, Yifeng Shi, and Daoyin Yu, Acoust. Phys. **63** (2), 229 (2017).
18. M. Albulayli and D. Rakhmatov, in *Proc. 2013 IEEE Int. Conference on Acoustics, Speech and Signal Processing (ICASSP)* (Vancouver, 2013), p. 1061.
19. O. L. Frost III, Proc. IEEE **60** (8), 926 (1972).
20. Murat Alparslan Gungor and Irfan Karagoz, IET Image Process. **11** (9), 667 (2017).
21. J. A. Jensen, in *Proc.10th Nordic-Baltic Conference on Biomedical Imaging* (Tampere, 1996), Vol. 4. Suppl. 1, Part 1, p. 351.
22. V. A. Zverev, Acoust. Phys. **62** (3), 383 (2016).
23. K. Dei, A. Luchies and B. Byram, in *Proc. 2017 IEEE Int. Ultrasonics Symposium (IUS)* (Washington, DC, 2017), p. 1.
24. Yang Lou and Jesse T. Yen, Ultrasonics **78**, 152 (2017).